Temporal stimulus patterns drive differentiation of a synthetic dipeptide-based coacervate

Ryou Kubota,[1]* Shogo Torigoe,[1] Itaru Hamachi[1,2]*

[1]Department of Synthetic Chemistry and Biological Chemistry, Graduate School of Engineering, Kyoto University, Katsura, Nishikyo-ku, Kyoto 615-8510, Japan

[2]JST-ERATO, Hamachi Innovative Molecular Technology for Neuroscience, Katsura, Nishikyo-ku, Kyoto 615-8530, Japan

Correspondence: rkubota@sbchem.kyoto-u.ac.jp, ihamachi@sbchem.kyoto-u.ac.jp

Abstract

The fate of living cells often depends on their processing of temporally modulated information, such as the frequency and duration of various signals. Synthetic stimulus-responsive systems have been intensely studied for >50 y, but it is still challenging for chemists to create artificial systems that can decode dynamically oscillating stimuli and respond in the systems' properties/functions, because of the lack of sophisticated reaction networks that are comparable with biological signal transduction. Here we report morphological differentiation of synthetic dipeptide-based coacervates in response to temporally distinct patterns of the light pulse. We designed a simple cationic diphenylalanine peptide derivative to enable formation of coacervates. The coacervates concentrated an anionic methacrylate monomer and a photo-initiator, which provided a unique reaction environment and facilitated light-triggered radical polymerization—even in air. Pulsed light irradiation at 9.0 Hz (but not at 0.5 Hz) afforded anionic polymers. This dependence on the light pulse patterns is attributable to the competition of reactive radical intermediates between the methacrylate monomer and molecular oxygen. The temporal pulse pattern-dependent polymer formation enabled the coacervates to differentiate in terms of morphology and internal viscosity, with an ultrasensitive switch-like mode. Our achievements will facilitate rational design of smart supramolecular soft materials and are insightful regarding synthesis of the sophisticated chemical cells.

Introduction

The fate of living cells, such as differentiation and apoptosis, depends on the extracellular environment.[1] The signals are varied as not only static information such as types and concentration of signalling molecules, but also dynamically modulated information in terms of frequency and duration.[2,3] Cells can decode temporally dynamic signals into different phenotypic responses by controlling gene expression patterns.[4–7] For example, T lymphocytes exhibit distinct immune responses (depending on the frequency of Ca^{2+} oscillation) through activation of different sets of transcription factors [Fig. 1a (i)].[4] Neuronal progenitor cells can maintain their multipotent state through oscillatory expression of three types of transcription factors, and differentiate into three distinct cell types (neurons, astrocytes, and microglia) when the expression patterns change from oscillatory to sustained [Fig. 1a (ii)].[7] To decipher temporal signalling dynamics, cells rely on sophisticated signalling networks composed of specific motifs, such as positive/negative feedbacks and feedforward loops of enzymes and transcriptional factors. Researchers hypothesize that such dynamic aspects of intracellular signal transduction enable transmission of rich and complex information—with a limited set of signalling molecules—in a robust manner.

Inspired by elegant biological systems, many chemists have focused on developing synthetic supramolecular systems (including molecular recognition and stimulus responses) for >50 years.[8–10] Stimulus-responsive supramolecular materials have potential applications in controlled drug delivery, biomedical sensing and diagnostics, and regenerative medicine.[11–13] However, artificial materials developed to date exhibit responses to static information, such as types and concentration of signals. Chemists unfortunately lack elaborate catalysts and sophisticated reaction networks that are comparable with biological machinery. It thus remains challenging to develop synthetic systems that can decode a temporally oscillating stimulus.

Here we report a synthetic coacervate that can differentiate in response to repeated pulse stimuli with distinct intervals (Fig. 1b). Coacervates are liquid-like membraneless molecular assemblies that form through liquid–liquid phase separation (LLPS).[14–16] Because of their ability to concentrate a wide variety of molecules and promote reactions in the interior, coacervates are a protocell model that may be pertinent to the origin of life.[17–31] This study demonstrates that only three key

components are needed to enable the temporally distinct stimulus pattern-dependent response of an artificial system: (i) synthetic coacervates composed of a simple cationic dipeptide, (ii) anionic polymers that are synthesized by stimuli-triggered radical polymerization inside the coacervates, and (iii) light with a tunable pulse frequency. Pulsed light-emitting diode (LED) irradiation at high frequency—to coacervates containing a photo-initiator and a methacrylate monomer—produced anionic polymers that strongly interacted with the cationic dipeptide, leading to changes in the morphology and physical properties of the coacervates. In contrast, no changes in the coacervates occurred by using pulsed light with a lower frequency. The mechanistic study reveals that this temporal pattern-dependent coacervate differentiation was induced by the presence/absence of *in situ* photo-generated polymers, which can be controlled by the substrate competition between molecular oxygen and the methacrylate monomer towards reactive radical intermediates. This differentiation also represents an ultrasensitive switch-like response that is rarely carried out in synthetic systems chemistry.[32]

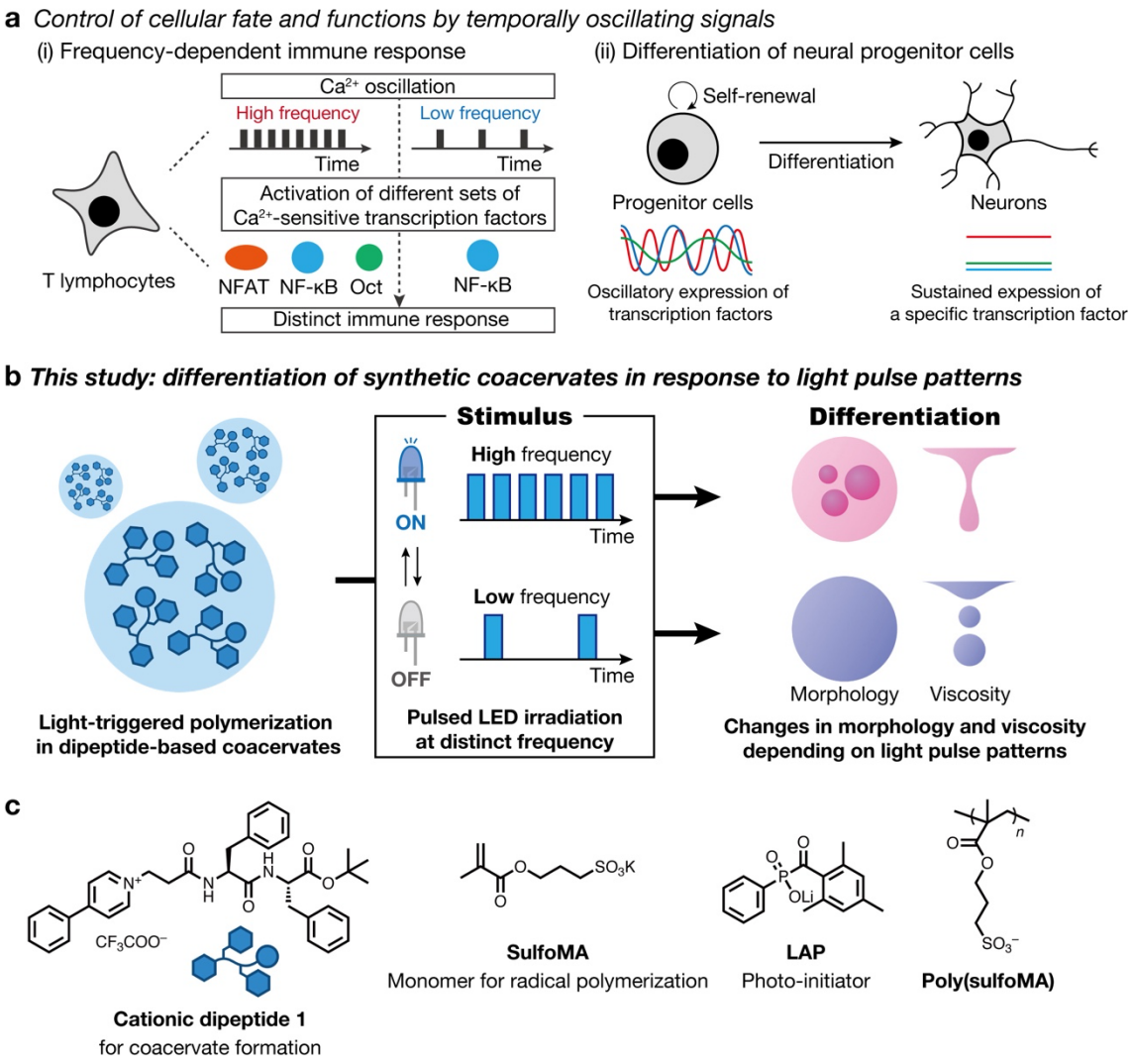

Fig. 1. Conceptual illustration of differentiation of synthetic coacervates driven by temporally oscillating stimuli. (**a**) Biological examples of control of cellular fate and functions by temporally oscillating signals. NFAT, NF-*κ*B, and Oct are transcription factors. NFAT: nuclear factor of activated T cells, NF-*κ*B: nuclear factor *κ*-light-chain-enhancer of activated B cells, Oct: octamer transcription factor. (**b**) Concept of this study: differentiation of synthetic dipeptide-based coacervates in response to temporally distinct patterns of the light pulse. (**c**) Chemical structures of a cationic dipeptide **1** for coacervate formation, a methacrylate monomer (sulfoMA) and a photo-initiator (LAP) for radical polymerization, and a poly(sulfoMA) polymer. SulfoMA: 3-sulfopropyl methacrylate potassium salt, LAP: lithium phenyl(2,4,6-trimethylbenzoyl)phosphinate.

Results and discussion

We designed a novel dipeptide derivative **1** that contains a *tert*-butyl phenylalanylphenylalaninate (FF–OtBu) motif as a key module for LLPS (Fig. 1c). A diphenylalanine sequence has been frequently used as a self-assembling moiety for supramolecular nanofibers and coacervates.[33–38] To avoid biased formation of nanofibers, we introduced a bulky *tert*-butyl group at the *C*-terminus. In addition, we attached a 4-phenylpyridinium group at the *N*-terminus to potentially induce cation–π interactions, which are often crucial for LLPS of biomacromolecules.[15,16]

We prepared a coacervate solution by heating dipeptide **1** in a 2-(*N*-morpholino)ethanesulfonic acid (MES) buffer (100 mM, pH 7.0), followed by cooling to room temperature to obtain a white suspension (Fig. 2a). By microscopic imaging, we observed many spherical droplets with a diameter of 2.8 ± 0.9 μm that exhibited sedimentation and coalescence into larger droplets, indicating their liquid-like properties (Figs. 2b, c, Fig. S1, Movie 1). The time-course of transparency measurement shows that sedimentation was completed within 3 h (Fig. S2). To estimate the fluidity of **1** in the droplets, we prepared a fluorescent probe by tethering BODIPY FL dye at the *N*-terminus of the FF–OtBu motif (**2**, Fig. S3). Fluorescence recovery after photobleaching (FRAP) analysis of coacervates containing **1** and **2** (0.067 mol% of **2** mixed with **1**) indicates rapid and almost complete recovery with a half time and mobile fraction of 4.08 ± 0.14 s and 83.2% ± 0.9%, respectively (Figs. 2d–f, Movie 2). We also conducted microrheological analysis to evaluate the viscosity of the coacervates, using carboxylate-modified polystyrene beads with a diameter of 1.0 μm as a probe. A log–log plot of mean square displacement against lag time indicates a slope of *ca.* 1, suggesting that the droplets behaved as a viscous liquid (Fig. 2g, Fig. S4).[39] In accordance with the Stokes–Einstein equation, we calculated the viscosity to be 4.08 ± 0.13 Pa·s, which is similar to that of jam and some *in vitro* protein-based coacervates.[40,41] These coacervates were stable in their liquid state on the glass surface for at least 28 d, as confirmed by time-lapse microscopic observations (Fig. S5). This outstanding long lifetime of our coacervates may be due to inhibition of β-sheet formation of the FF peptide through the bulky tBu group at the *C*-terminus, as expected.[42] In accordance with transparency measurements, the coacervates exhibited temperature-dependent assembly–disassembly with a melting temperature of *ca.* 56ºC,

over at least three cycles between 20ºC and 60ºC (Fig. S6). We determined the critical coacervation concentration to be between 3 and 10 mM (Fig. S7). These data reveal that the designer dipeptide **1** self-assembled into stable coacervates by LLPS.

We subsequently investigated uptake of several fluorescent dyes bearing diverse properties: fluorescein, Nile red, rhodamine B (RhoB), and rhodamine 6G (Rho6G). Confocal microscopy images of the coacervates after adding the fluorescent dyes demonstrated substantially strong fluorescence inside the coacervates, indicating that all of the dyes were concentrated inside the coacervates (Fig. 2h, Fig. S8). We quantitatively determined the quantities of the encapsulated dyes by high-performance liquid chromatography (HPLC) and fluorescence spectroscopy analysis of the supernatant (Fig. S9). The estimated partition coefficients indicate that the coacervates were enriched in anionic fluorescein and hydrophobic Nile red more efficiently than in zwitterionic RhoB and cationic Rho6G (Fig. 2h). These results indicate that both electrostatic and hydrophobic interactions between the assembled **1** and fluorescent dyes may be the driving forces for molecular sequestration.

Using the molecular uptake capability, we performed peptide oligomerization inside the coacervates by using a hydrophobic *N*-carboxy anhydride of L-phenylalanine (L-Phe NCA) as a monomer and anionic FL–NH_2 as an initiator (Fig. 2i). NCA derivatives are a plausible prebiotic active species for peptide synthesis.[20,43,44] To our best knowledge, however, no attempts have been made to use NCA derivatives for a reaction inside coacervates. Because of the relatively fast hydrolysis of NCA (0.018 s^{-1} at pH 8.5) in aqueous solution,[44] the desired peptide formation should compete against nonproductive NCA hydrolysis. However, we expected that the oligomerization reaction could preferentially proceed inside the coacervates through concurrent sequestration of FL–NH_2 and L-Phe NCA (Fig. S10). HPLC analysis 3 h after adding L-Phe NCA into a mixture of the coacervate and FL–NH_2 indicate that 84.7% ± 0.6% of FL–NH_2 was consumed and we observed signals attributable to Phe-oligomers (FL–Phe_n: n = 1–4; Fig. 2j, Fig. S11). The calibration curves indicate that the number-average degree of polymerization (DP_n) and dispersity were 1.77 ± 0.09 and 1.38 ± 0.02, respectively (Fig. S12). In contrast, only 7.3% ± 0.2% of the FL–NH_2 reacted; we detected weak signals of FL–Phe_1 and an almost negligible quantity of FL–Phe_2 in the absence of the coacervates (DP_n: 0.092 ± 0.004). These data demonstrate that the coacervates can

provide a unique microenvironment that favourably promotes plausible prebiotic peptide oligomerization by suppressing the competitive NCA hydrolysis.

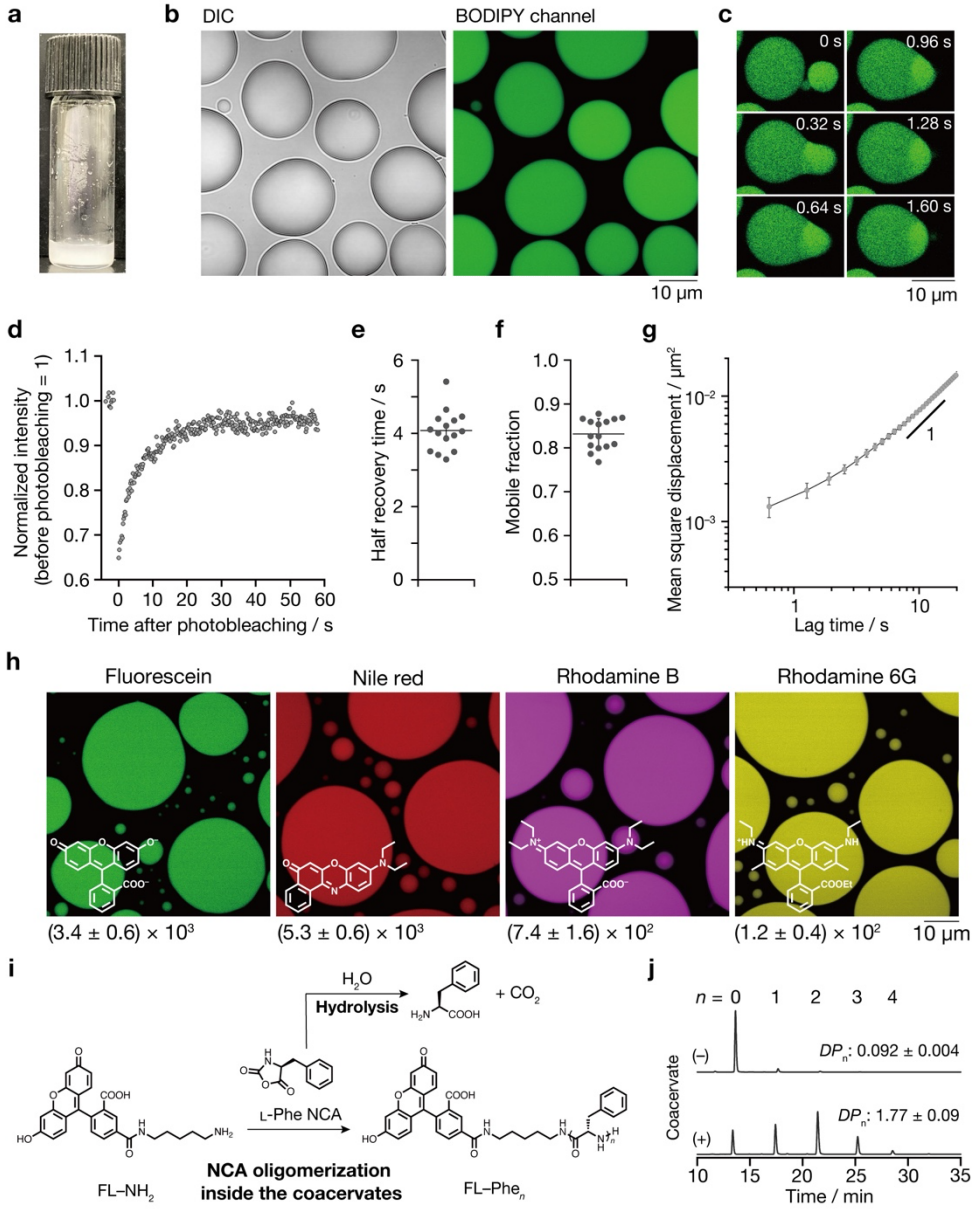

Fig. 2. Liquid–liquid phase separation of a synthetic cationic dipeptide. (**a**) Photograph of a suspension containing coacervate droplets. (**b**) Confocal laser scanning microscopy (CLSM) images of the coacervates containing **1** and the fluorescent probe **2**. Chemical structure of **2** is shown in Fig. S3. Left: Differential interference contrast (DIC) image, right: BODIPY channel. (**c**) Time-lapse CLSM images of coalescence of the coacervates. (**d**) FRAP analysis of the coacervates containing **1** and **2**. The representative data is shown. (**e**) Half recovery time and (**f**) mobile fraction of **2**. The data represent the mean ± standard error of the mean (s.e.m.) (n = 15). (**g**) Microrheological analysis of the coacervates. The slope of a black solid line is 1. The

data represent the mean ± s.e.m. (n = 60). (**h**) CLSM images of fluorescent dye uptake into the coacervates. Insets show chemical structures of fluorescent dyes, and the numbers shown below the images are partition coefficients (K_p: defined as [concentration in the coacervate]/[concentration in the supernatant]). (**i**) Schematic illustration of peptide oligomerization with L-Phe NCA and FL–NH_2 as a monomer and an initiator, respectively. Competitive hydrolysis of NCA concurrently proceeds in aqueous solution. NCA: *N*-carboxy anhydride. (**j**) HPLC charts of the reaction mixtures in the (top) absence and (bottom) presence of the coacervates. The data represent the mean ± standard deviation (s.d.) (n = 3). Condition: [**1**] = 15 mM, [**2**] = 10 μM (for **b**–**f**), [fluorescein] = [Nile Red] = [rhodamine B] = [rhodamine 6G] = 10 μM (for **h**), [FL–NH_2] = 1.0 μM (for **j**), [L-Phe NCA] = 200 μM (for **j**), 100 mM MES, pH 7.0, 23ºC (for **d**–**f**), 24ºC (for **g**), rt, 3 h (for **j**).

With the coacervates as a unique reaction environment, we next conducted light-triggered radical polymerization inside the coacervates by using an anionic methacrylate monomer and a photo-initiator. Generally speaking, the radical polymerization—in terms of its efficiency (*e.g.*, yield and degree of polymerization)—depends on molecular oxygen, a competitive quencher for the active radical intermediates. We expected either coacervates or the light pulse (temporal) pattern might impact the polymerization under such competitive conditions. We also anticipated that the produced anionic polymers would facilitate alteration of the coacervate properties through enhanced electrostatic interactions with cationic dipeptide **1**.[45] We used 3-sulfopropyl methacrylate potassium salt (sulfoMA) and lithium phenyl(2,4,6-trimethylbenzoyl)phosphinate (LAP) as an anionic monomer and a photo-initiator, respectively (Fig. 1c). HPLC analysis indicates that both sulfoMA and LAP were concentrated in the coacervates (Fig. S13). After adding a mixture of sulfoMA and LAP to a suspension containing the coacervates in a MES D_2O buffer (100 mM, pD 7.0), we irradiated continuous LED light (λ_{max}: 365 nm, 23.5 mW/cm^2) for 10 min in air (Fig. S14). We then dissolved the resulting mixture in methanol-d_4 and analyzed the mixture by ^{1}H nuclear magnetic resonance (NMR) spectroscopy. ^{1}H NMR spectra indicate that 25% ± 3% of the sulfoMA monomer was consumed and we detected signals that are attributable to the poly(sulfoMA) polymer (Figs. S15b, S16). In accordance with size-exclusion chromatography (SEC), the number-average molecular weight and DP_n were (3.3 ± 0.2) × 10^4 and 82 ± 11, respectively (Fig. S17a) [determined by using polyethylene glycol (PEG) and poly(sulfoMA) standards, respectively; see Supporting Information for details: Fig. S18]. As controls, we obtained no polymer products without either LED irradiation or the photo-initiator (Figs. S15c, d). To confirm if the radical polymerization proceeded inside the coacervates, we performed LED irradiation of the supernatant after centrifugation. ^{1}H NMR spectra indicate that we did not produce any polymers, and thus light-triggered radical polymerization proceeded inside the coacervates (Fig. S19).

We next carried out pulsed LED irradiation of the coacervates in the presence of sulfoMA and LAP. We controlled the frequency of the LED light pulse by changing the OFF time (an interval time of 11–1900 ms) under a constant ON time (100 ms) with identical pulse numbers (3000 times) (Fig. 3a, Movie 3). The consumption ratio of sulfoMA determined by ^{1}H NMR measurements was substantially distinct, depending

on the irradiation patterns (7% ± 3% and 22% ± 2% for 0.5- and 9.0-Hz irradiation, respectively; Figs. 3b, 3d, Fig. S20). We observed signals that are attributable to the polymers in the 9.0-Hz irradiated sample, but not in the 0.5-Hz irradiated sample. SEC analyses indicate that the DP_n of the polymers at 9.0-Hz irradiation was 63 ± 5 (dispersity: 1.85 ± 0.08), whereas there was almost no peak for the 0.5-Hz irradiation (Figs. 3c, 3d, Figs. S17b, c). These data reveal that the efficiency of light-triggered radical polymerization was substantially dependent on the photo-irradiation pulse patterns, albeit at the same irradiation dose.

To examine the impacts of molecular oxygen and the coacervates on this radical polymerization, we conducted three additional experiments. The first experiment was photo-polymerization with a 0.5-Hz pulse frequency in an Ar atmosphere (Fig. S21). The yield was substantially increased: 47% ± 9% (Figs. 3b, 3d, Fig. S22); and the number-average molecular weight and dispersity of the obtained polymers were (4.3 ± 0.9) × 10^4 and 2.10 ± 0.05, respectively (Figs. 3c, 3d, Fig. S17d). Furthermore, the irradiation patterns showed a negligible impact on the polymerization in an Ar atmosphere [yield: 37% ± 12%, the number-average molecular weight and dispersity of polymerization: (2.90 ± 0.14) × 10^4 and 1.72 ± 0.07, respectively, for a 9.0-Hz pulse frequency] (Figs. S17e, S22). These data indicate that molecular oxygen was a strong inhibitor of the radical polymerization inside the coacervates and played important roles on the pulse pattern dependency in air. The second experiment was radical polymerization without the coacervates using 9.0-Hz of pulse frequency in air. There was monomer (sulfoMA) consumption (24% ± 3%, Fig. S23) by ^{1}H NMR measurements, but the SEC curve substantially shifted to the lower molecular weight region compared with that obtained in the presence of the coacervates (Fig. 3c, Fig. S24). The third experiment was radical polymerization in a buffer, where concentrations of sulfoMA and LAP were identical with those in the coacervate (sulfoMA: 190 mM, LAP: 25 mM). ^{1}H NMR measurements showed 87.7% ± 0.8% of sulfoMA was consumed, but the estimated number-average molecular weight (5480 ± 60) was 5-fold smaller than that in the presence of the coacervate (Figs. S25 and S26). Clearly, our coacervates can promote radical polymerization even in O_2-rich competitive conditions, probably through enrichment of both the sulfoMA monomer and LAP inside the coacervates and suppression of termination reactions.

Combined with these results, it is conceivable that the competition of reactive radical species between the sulfoMA monomer and molecular oxygen is critical for the dependence of the polymerization on the photo-irradiation pulse patterns (Fig. 3e). In open-air reaction systems, molecular oxygen diffuses from the air and dissolves into the aqueous phase and coacervates. The quantity of radicals photo-generated per unit time depends on the OFF time of the light pulse. At photoirradiation with the longer OFF time (0.5 Hz), the generated radicals are small in quantity and thus effectively quenched by the dissolved molecular oxygen. However, when irradiated with the shorter OFF time (9.0 Hz), the quantity of the radicals photo-generated per unit time is greater than that in the longer OFF time case, such that the radicals can escape from the quenching by using molecular oxygen, leading to enhanced formation of poly(sulfoMA) polymers.

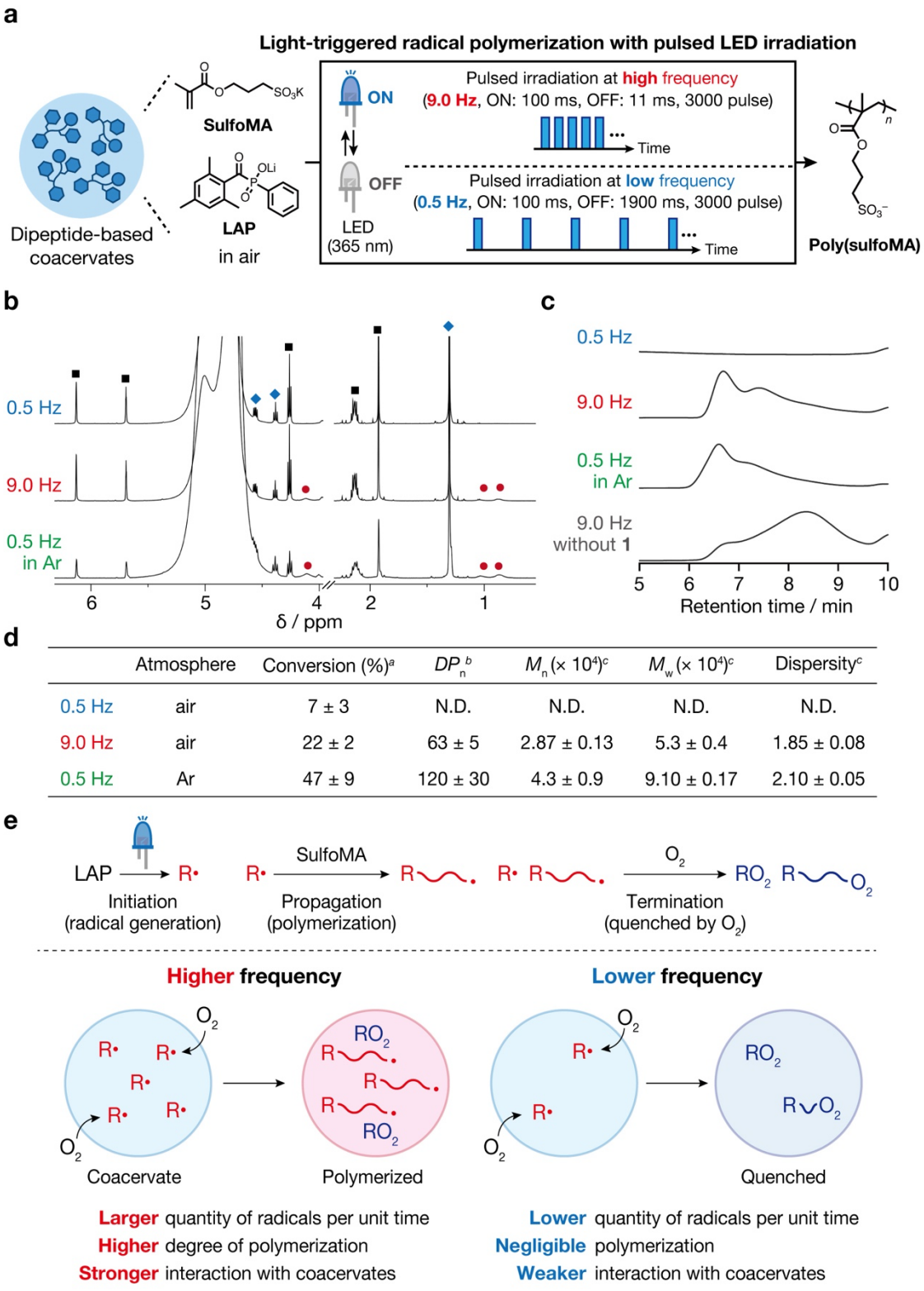

	Atmosphere	Conversion (%)[a]	DP_n[b]	M_n (× 10^4)[c]	M_w (× 10^4)[c]	Dispersity[c]
0.5 Hz	air	7 ± 3	N.D.	N.D.	N.D.	N.D.
9.0 Hz	air	22 ± 2	63 ± 5	2.87 ± 0.13	5.3 ± 0.4	1.85 ± 0.08
0.5 Hz	Ar	47 ± 9	120 ± 30	4.3 ± 0.9	9.10 ± 0.17	2.10 ± 0.05

Fig. 3. Radical polymerization triggered by pulsed light irradiation in the coacervates. (**a**) Schematic illustration of radical polymerization inside the coacervate triggered by pulsed LED irradiation. (**b**) ^{1}H NMR spectra (500 and 400 MHz, 4:6 D_2O/CD_3OD, rt)

after pulsed LED irradiation. Black square: sulfoMA, blue rhombus: dipeptide **1**, red circle: poly(sulfoMA) polymer. (**c**) SEC charts after pulsed LED irradiation. (**d**) Table of ^{1}H NMR and SEC data. N.D.: not determined, *a*: determined by ^{1}H NMR, *b*: estimated by SEC with a calibration curve using poly(sulfoMA) polymers synthesized by RAFT polymerization, *c*: determined by SEC with PEG standards. The data represent the mean ± s.d. (n = 3). Reaction condition: [**1**] = 15 mM, [**2**] = 10 μM, [sulfoMA] = 15 mM, [LAP] = 0.3 mM in 100 mM MES (pH 7.0). (**e**) Plausible mechanism of dependence of light pulse patterns in radical polymerization. R (red) and RO_2 (dark blue) mean reactive radical intermediates and quenched molecules/polymers by O_2, respectively. Other termination mechanisms such as combination and disproportionation of the radicals were omitted for clarity.

The morphologies/properties of the coacervates changed during pulsed-light-triggered polymerization (Fig. 1b). Confocal microscopy images indicate that many droplets with a diameter ranging from 0.26–1.9 μm (0.8 ± 0.3 μm) were generated inside the coacervates after 9.0-Hz light pulse irradiation (Fig. 4a, left). These inner droplets exhibited coalescence, indicating their liquid-like nature (Fig. S27, Movie 4).[46–48] These inner droplets showed growth by adding H_2O, whereas these temporally disappeared by addition of saturated NaCl aqueous solution, which suggest the droplets may be formed through tight electrostatic interaction between **1** and poly(sulfoMA) polymers (Fig. S28). In contrast, the morphology remained unchanged and we did not observe inner droplets after 0.5-Hz light pulse irradiation, albeit at the same photo-irradiation dose (Fig. 4a, right). FRAP analysis demonstrated that the physical properties of the coacervate changed after pulsed light irradiation in a pulse pattern-dependent manner. In the case of the 0.5-Hz pulse irradiated coacervates, we observed rapid recovery with a half time and mobile fraction of 6.3 ± 0.2 s and 67.4% ± 0.5%, respectively; which are almost comparable with those of nonirradiated coacervates (5.93 ± 0.07 s and 68.4% ± 0.2%, respectively) (Figs. 4b–d, blue and black, respectively; Movie 5). However, the coacervates after 9.0-Hz pulse irradiation exhibited a substantially distinct recovery profile: a longer half time and lower mobile fraction of 11.7 ± 0.3 s and 42.1% ± 0.7%, respectively (Figs. 4b–d, red, Movie 5). Microrheological analysis gave almost the same viscosity between the nonirradiated and 0.5-Hz irradiated coacervates (3.81 ± 0.19 and 3.66 ± 0.13 Pa·s, respectively; Fig. S4, black and blue, respectively). In the 9.0-Hz irradiated coacervates, in contrast, microbeads exhibited little Brownian motion, indicating its much higher viscosity than the nonirradiated and 0.5-Hz irradiated coacervates (Fig. S4a, red). It is reasonable to hypothesize that such increased gel-like viscosity is attributable to the tighter electrostatic interactions of cationic **1** with the anionic polymers that were efficiently generated inside the coacervates with the 9.0-Hz pulse irradiation (Figs. 1b, 3e). Taken together, the dipeptide-based coacervates can differentiate in terms of morphology and physical properties, in response to temporally distinct light pulse patterns.

We finally examined such stimuli-pattern dependence in detail, by confocal imaging and FRAP measurements of the differentiated coacervates. The morphological change occurred with 2.0 Hz or more of pulse frequency (Fig. S29). Interestingly, the

responses in terms of both the half recovery time and mobile fraction exhibited a sigmoid-shaped curve, reaching a plateau at 4.0 Hz (Fig. 4e, Fig. S30). This nonlinear response was well-approximated by a Hill equation: Hill coefficients of 3.4 and 2.4 for half recovery time and mobile fraction, respectively, indicating that this synthetic coacervate system exhibited an ultrasensitive response to the temporally distinct patterns of the light pulse. The ultrasensitive response of the coacervates in our work is attributable to competition of the reactive radicals between the methacrylate monomer and molecular oxygen.[49,50] As described above, molecular oxygen diffused from the air effectively quenches reactive radical species at lower frequency to generate a threshold, whereas the amount of the radicals produced at higher frequency becomes higher than that of molecular oxygen to proceed radical polymerization, resulting in the ultrasensitive response. Such the ultrasensitive response based on the competitive mechanism is considered as a new example of light-fueled dissipative systems.[28,51–72] To date, it has been reported that coacervates can provide a microenvironment to accelerate catalytic reactions mainly through molecular sequestration[25,73–85] and to realize stimulus responses towards reactive molecules (*e.g.* assembly-disassembly).[24,28,38,45,82,86–90] Compared with these examples, one of the important aspects of our work is to combine the rate enhancement effect with competitive inhibition via continuous supply of diffusing O_2, which establishes a unique system in response to temporally distinct stimulus patterns. The similar ultrasensitive responses were recently enabled by coupling of enzymatic reactions with artificial photo-responsive inhibitors in a flow reactor, but are still rare in synthetic systems chemistry.[91]

We further performed FRAP experiments to confirm if our light responsive system can discriminate (i) between the continuous/pulsed irradiation and (ii) among the pulse frequencies under the condition where the time-averaged light intensity and the total light intensity are constant (Fig. S31). FRAP analysis of the samples treated with continuous and 9.0-Hz pulsed irradiation demonstrated the difference in the mobile fraction (25.6% ± 1.8% and 33% ± 2%, respectively). Also, the mobile fraction of the sample with 5.0-Hz pulsed irradiation (27% ± 2%) was lower than that of 9.0-Hz pulsed irradiation. Taken together, it is considered that our light responsive system can finely control its response by distinguishing temporally distinct photo-stimuli patterns, although the time-average light intensity should be the main controlling factor of the

light responsive system.

The present results demonstrate induction of differentiation of synthetic dipeptide-based coacervates driven by temporally distinct stimulus dynamics. The proposed system, which can decode dynamic (temporal) information, is applicable to a wide variety of synthetic stimulus-responsive supramolecules because it relies on a simple, general substrate competition mechanism. Moreover, we found that our coacervate can accumulate enhanced green fluorescent protein (EGFP) selectively on its surface (Fig. S32, S33). Such unusual protein localization would lead to construction of unique compartmentalized enzymatic networks, which might be useful for decoration of coacervate surface through enzymatic polymer synthesis toward potential application such as drug delivery carriers. We expect that the release rate of encapsulated drugs/proteins from the coacervate carriers would be controlled by tuning the inner viscosity with the unique light response. Further development will facilitate intelligent chemical cells that enable life-like complex information processing.

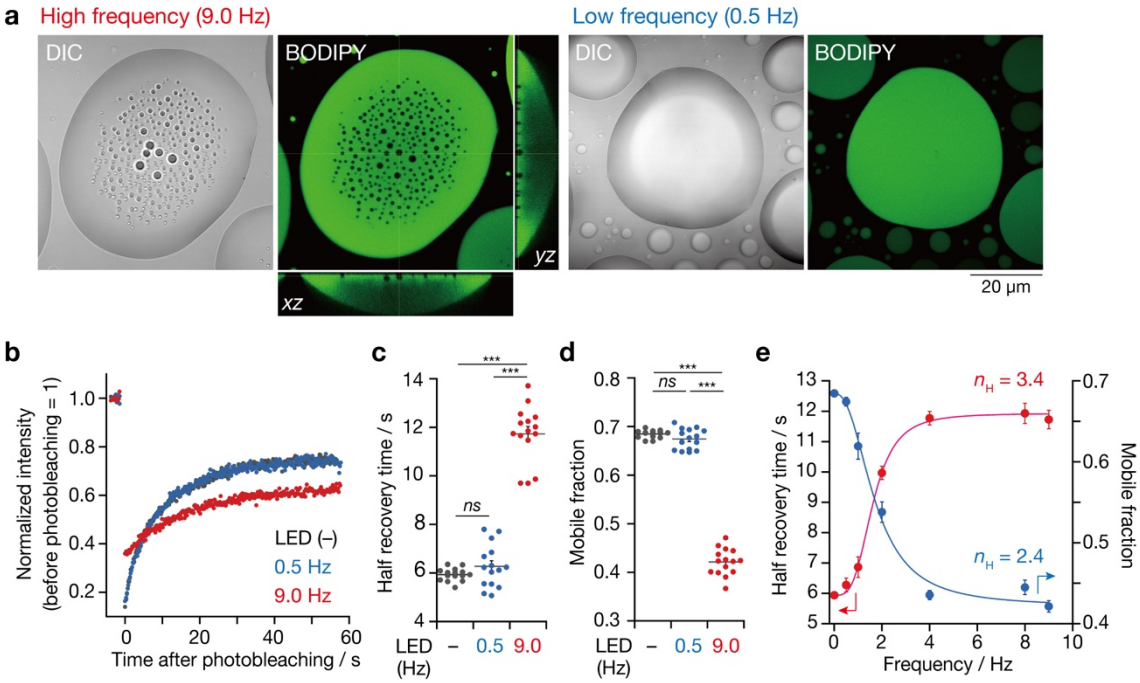

Fig. 4. Differentiation of the coacervates in response to the temporally distinct patterns of the light pulse. (**a**) CLSM images of the coacervates after pulsed LED irradiation (left: 9.0 Hz, right: 0.5 Hz). (**b**) FRAP analysis of the coacervates with/without pulsed light irradiation. (**c**) Half recovery time and (**d**) mobile fraction of **2**. Black: without irradiation [LED(–)], blue: 0.5 Hz, red: 9.0 Hz. (**e**) Plot of (red) half recovery time and (blue) mobile fraction against light pulse frequency. The responses were fitted by a Hill equation. n_H: Hill coefficient. Condition: [**1**] = 15 mM, [**2**] = 10 μM, [sulfoMA] = 15 mM, [LAP] = 0.3 mM in 100 mM MES (pH 7.0). The data represent the mean ± s.e.m. (n = 15). *Post hoc* multiple comparisons were conducted using a one-way ANOVA followed by Tukey's test. ***: $P < 0.001$. *ns*: not significant.

ASSOCIATED CONTENT

Supporting information

The Supporting Information is available free of charge at https://pubs.acs.org/doi/10.1021/jacs.xxxxx. The authors declare that the data supporting the finding of this study are available with the paper and its Supporting Information files and from the corresponding author upon reasonable request.

Description of materials, experimental methods, organic synthesis and compound characterization, microscopic observation of the coacervates, chemical structure of the fluorescent probe, microrheological analysis, temperature-dependent transparency measurement, uptake of fluorescent dyes, sulfoMA, and LAP, HPLC analysis of oligomerization of L-Phe NCA, ^{1}H NMR spectra after radical polymerization, SEC charts of poly(sulfoMA) polymers, FRAP analysis after LED irradiation (PDF)

Movie of time-lapse microscopic imaging of the coacervates. Condition: [**1**] = 15 mM, 100 mM MES, pH 7.0, rt. Elapsed time was displayed as mm:ss (AVI)

Movie of FRAP analysis of the coacervates containing fluorescent probe **2** as a fluorescent probe. Condition: [**1**] = 15 mM, [**2**] = 10 μM, 100 mM MES, pH 7.0, rt. Elapsed time was displayed as sec (AVI)

Movie of pulsatile LED irradiation to the coacervates (AVI)

Movie of Time-lapse microscopic imaging of coalescence of the inner droplets inside the coacervates after LED irradiation at 9.0 Hz. Elapsed time was displayed as sec. (AVI)

Movie of FRAP analysis of the coacervates containing fluorescent probe **2**, sulfoMA, and LAP (top) without LED irradiation and after LED irradiation at (middle) 0.5 and (bottom) 9.0 Hz in air. Condition: [**1**] = 15 mM, [**2**] = 10 μM, [sulfoMA] = 15 mM, [LAP] = 0.3 mM, 100 mM MES, pH 7.0, rt. Elapsed time was displayed as sec (AVI)

AUTHOR INFORMATION

Corresponding authors

Ryou Kubota –*Department of Synthetic Chemistry and Biological Chemistry, Graduate*

School of Engineering, Kyoto University, Katsura, Nishikyo-ku, Kyoto 615-8510, Japan; orcid.org/0000-0001-8112-8169; Email: rkubota@sbchem.kyoto-u.ac.jp

Itaru Hamachi – *Department of Synthetic Chemistry and Biological Chemistry, Graduate School of Engineering, Kyoto University, Katsura, Nishikyo-ku, Kyoto 615-8510, Japan; JST-ERATO, Hamachi Innovative Molecular Technology for Neuroscience, Nishikyo-ku, Kyoto 615-8530, Japan;* orcid.org/0000-0002-3327-3916; Email: ihamachi@sbchem.kyoto-u.ac.jp

Author

Shogo Torigoe – *Department of Synthetic Chemistry and Biological Chemistry, Graduate School of Engineering, Kyoto University, Katsura, Nishikyo-ku, Kyoto 615-8510, Japan*

NOTE

Authors declare no competing interests.

ACKNOWLEDGEMENTS

We appreciate Ms. Risa Hatazawa of her assistance for SEC measurements. This work was supported by a Grant-in-Aid for Scientific Research on Innovative Areas "Chemistry for Multimolecular Crowding Biosystems" (JSPS KAKENHI Grant JP17H06348), the Japan Science and Technology Agency (JST) ERATO Grant Number JPMJER1802 to I.H., and by a Grant-in-Aid for Young Scientists (JSPS KAKENHI Grant JP20K15400) and a Grant-in-Aid for Scientific Research (B) (JSPS KAKENHI Grant JP22H02195) to R.K., and by JST Spring Grant Number JPMJSP2110 to S.T. We thank Michael Scott Long, PhD, from Edanz (https://jp.edanz.com/ac) for editing a draft of this manuscript.

REFERENCES

(1) Alberts, B (eds). *Molecular Biology of the Cell* 6th edn; Garland Science, 2016.

(2) Kholodenko, B. N.; Hancock, J. F.; Kolch, W. Signalling Ballet in Space and Time. *Nat. Rev. Mol. Cell Biol.* **2010**, *11*, 414–426.

(3) Purvis, J. E.; Lahav, G. Encoding and Decoding Cellular Information through Signaling Dynamics. *Cell* **2013**, *152*, 945–956.

(4) Dolmetsch, R. E.; Xu, K.; Lewis, R. S. Calcium Oscillations Increase the Efficiency and Specificity of Gene Expression. *Nature* **1998**, *392*, 933–936.

(5) Cai, L.; Dalal, C. K.; Elowitz, M. B. Frequency-Modulated Nuclear Localization Bursts Coordinate Gene Regulation. *Nature* **2008**, *455*, 485–490.

(6) Ashall, L.; Horton, C. A.; Nelson, D. E.; Paszek, P.; Harper, C. V.; Sillitoe, K.; Ryan, S.; Spiller, D. G.; Unitt, J. F.; Broomhead, D. S.; Kell, D. B.; Rand, D. A.; Sée, V.; White, M. R. H. Pulsatile Stimulation Determines Timing and Specificity of NF-κB-Dependent Transcription. *Science* **2009**, *324*, 242–246.

(7) Imayoshi, I.; Isomura, A.; Harima, Y.; Kawaguchi, K.; Kori, H.; Miyachi, H.; Fujiwara, T.; Ishidate, F.; Kageyama, R. Oscillatory Control of Factors Determining Multipotency and Fate in Mouse Neural Progenitors. *Science* **2013**, *342*, 1203–1208.

(8) Pedersen, C. J. Cyclic Polyethers and Their Complexes with Metal Salts. *J. Am. Chem. Soc.* **1967**, *89*, 7017–7036.

(9) Steed, J. W.; Atwood, J. L. *Supramolecular Chemistry* 2nd edn, Wiley, 2009.

(10) Lehn, J.-M. Perspectives in Chemistry–Aspects of Adaptive Chemistry and Materials. *Angew. Chem. Int. Ed.* **2015**, *54*, 3276–3289.

(11) Webber, M. J.; Appel, E. A.; Meijer, E. W.; Langer, R. Supramolecular Biomaterials. *Nat. Mater.* **2016**, *15*, 13–26.

(12) Shigemitsu, H.; Hamachi, I. Design Strategies of Stimuli-Responsive Supramolecular Hydrogels Relying on Structural Analyses and Cell-Mimicking Approaches. *Acc. Chem. Res.* **2017**, *50*, 740–750.

(13) Culver, H. R.; Clegg, J. R.; Peppas, N. A. Analyte-Responsive Hydrogels: Intelligent Materials for Biosensing and Drug Delivery. *Acc. Chem. Res.* **2017**, *50*, 170–178.

(14) Aumiller, W. M., Jr; Keating, C. D. Experimental Models for Dynamic

Compartmentalization of Biomolecules in Liquid Organelles: Reversible Formation and Partitioning in Aqueous Biphasic Systems. *Adv. Colloid Interface Sci.* **2017**, *239*, 75–87.

(15) Abbas, M.; Lipiński, W. P.; Wang, J.; Spruijt, E. Peptide-Based Coacervates as Biomimetic Protocells. *Chem. Soc. Rev.* **2021**, *50*, 3690–3705.

(16) Shin, Y.; Brangwynne, C. P. Liquid Phase Condensation in Cell Physiology and Disease. *Science* **2017**, *357*, eaaf4382.

(17) Oparin, A. I. Evolution of the Concepts of the Origin of Life. *Orig. Life* **1976**, *7*, 3–8.

(18) Dzieciol, A. J.; Mann, S. Designs for Life: Protocell Models in the Laboratory. *Chem. Soc. Rev.* **2012**, *41*, 79–85.

(19) Buddingh', B. C.; van Hest, J. C. M. Artificial Cells: Synthetic Compartments with Life-like Functionality and Adaptivity. *Acc. Chem. Res.* **2017**, *50*, 769–777.

(20) Frenkel-Pinter, M.; Samanta, M.; Ashkenasy, G.; Leman, L. J. Prebiotic Peptides: Molecular Hubs in the Origin of Life. *Chem. Rev.* **2020**, *120*, 4707–4765.

(21) Menger, F. M.; Peresypkin, A. V. A Combinatorially-Derived Structural Phase Diagram for 42 Zwitterionic Geminis. *J. Am. Chem. Soc.* **2001**, *123*, 5614–5615.

(22) Imura, T.; Yanagishita, H.; Kitamoto, D. Coacervate Formation from Natural Glycolipid: One Acetyl Group on the Headgroup Triggers Coacervate-to-Vesicle Transition. *J. Am. Chem. Soc.* **2004**, *126*, 10804–10805.

(23) Dora Tang, T.-Y.; Rohaida Che Hak, C.; Thompson, A. J.; Kuimova, M. K.; Williams, D. S.; Perriman, A. W.; Mann, S. Fatty Acid Membrane Assembly on Coacervate Microdroplets as a Step towards a Hybrid Protocell Model. *Nat. Chem.* **2014**, *6*, 527–533.

(24) Aumiller, W. M., Jr; Keating, C. D. Phosphorylation-Mediated RNA/Peptide Complex Coacervation as a Model for Intracellular Liquid Organelles. *Nat. Chem.* **2016**, *8*, 129–137.

(25) Mason, A. F.; Buddingh', B. C.; Williams, D. S.; van Hest, J. C. M. Hierarchical Self-Assembly of a Copolymer-Stabilized Coacervate Protocell. *J. Am. Chem. Soc.* **2017**, *139*, 17309–17312.

(26) Douliez, J.-P.; Martin, N.; Gaillard, C.; Beneyton, T.; Baret, J.-C.; Mann, S.; Beven, L. Catanionic Coacervate Droplets as a Surfactant-Based Membrane-Free

Protocell Model. *Angew. Chem. Int. Ed.* **2017**, *56*, 13689–13693.
(27) Tian, L.; Li, M.; Patil, A. J.; Drinkwater, B. W.; Mann, S. Artificial Morphogen-Mediated Differentiation in Synthetic Protocells. *Nat. Commun.* **2019**, *10*, 3321.
(28) Donau, C.; Späth, F.; Sosson, M.; Kriebisch, B. A. K.; Schnitter, F.; Tena-Solsona, M.; Kang, H.-S.; Salibi, E.; Sattler, M.; Mutschler, H.; Boekhoven, J. Active Coacervate Droplets as a Model for Membraneless Organelles and Protocells. *Nat. Commun.* **2020**, *11*, 5167.
(29) Bhattacharya, A.; Niederholtmeyer, H.; Podolsky, K. A.; Bhattacharya, R.; Song, J.-J.; Brea, R. J.; Tsai, C.-H.; Sinha, S. K.; Devaraj, N. K. Lipid Sponge Droplets as Programmable Synthetic Organelles. *Proc. Natl. Acad. Sci. U. S. A.* **2020**, *117*, 18206–18215.
(30) Matsuo, M.; Kurihara, K. Proliferating Coacervate Droplets as the Missing Link between Chemistry and Biology in the Origins of Life. *Nat. Commun.* **2021**, *12*, 5487.
(31) Ianeselli, A.; Tetiker, D.; Stein, J.; Kühnlein, A.; Mast, C. B.; Braun, D.; Dora Tang, T.-Y. Non-Equilibrium Conditions inside Rock Pores Drive Fission, Maintenance and Selection of Coacervate Protocells. *Nat. Chem.* **2022**, *14*, 32–39.
(32) Ashkenasy, G.; Hermans, T. M.; Otto, S.; Taylor, A. F. Systems Chemistry. *Chem. Soc. Rev.* **2017**, *46*, 2543–2554.
(33) Sheehan, F.; Sementa, D.; Jain, A.; Kumar, M.; Tayarani-Najjaran, M.; Kroiss, D.; Ulijn, R. V. Peptide-Based Supramolecular Systems Chemistry. *Chem. Rev.* **2021**, *121*, 13869–13914.
(34) Reches, M.; Gazit, E. Casting Metal Nanowires within Discrete Self-Assembled Peptide Nanotubes. *Science* **2003**, *300*, 625–627.
(35) Yang, Z.; Liang, G.; Wang, L.; Xu, B. Using a Kinase/Phosphatase Switch to Regulate a Supramolecular Hydrogel and Forming the Supramolecular Hydrogel in Vivo. *J. Am. Chem. Soc.* **2006**, *128*, 3038–3043.
(36) Ikeda, M.; Tanida, T.; Yoshii, T.; Hamachi, I. Rational Molecular Design of Stimulus-Responsive Supramolecular Hydrogels Based on Dipeptides. *Adv. Mater.* **2011**, *23*, 2819–2822.
(37) Yuan, C.; Levin, A.; Chen, W.; Xing, R.; Zou, Q.; Herling, T. W.; Challa, P. K.; Knowles, T. P. J.; Yan, X. Nucleation and Growth of Amino Acid and Peptide

Supramolecular Polymers through Liquid-Liquid Phase Separation. *Angew. Chem. Int. Ed.* **2019**, *58*, 18116–18123.

(38) Abbas, M.; Lipiński, W. P.; Nakashima, K. K.; Huck, W. T. S.; Spruijt, E. A Short Peptide Synthon for Liquid-Liquid Phase Separation. *Nat. Chem.* **2021**, *13*, 1046–1054.

(39) Elbaum-Garfinkle, S.; Kim, Y.; Szczepaniak, K.; Chen, C. C.-H.; Eckmann, C. R.; Myong, S.; Brangwynne, C. P. The Disordered P Granule Protein LAF-1 Drives Phase Separation into Droplets with Tunable Viscosity and Dynamics. *Proc. Natl. Acad. Sci. U. S. A.* **2015**, *112*, 7189–7194.

(40) Zhang, H.; Elbaum-Garfinkle, S.; Langdon, E. M.; Taylor, N.; Occhipinti, P.; Bridges, A. A.; Brangwynne, C. P.; Gladfelter, A. S. RNA Controls PolyQ Protein Phase Transitions. *Mol. Cell* **2015**, *60*, 220–230.

(41) Folkmann, A. W.; Putnam, A.; Lee, C. F.; Seydoux, G. Regulation of Biomolecular Condensates by Interfacial Protein Clusters. *Science* **2021**, *373*, 1218–1224.

(42) A diphenylalanine (FF) motif is widely used as a self-assembling moiety for synthetic supramolecular nanofibers with a β-sheet type packing structure. In 2019, Yuan and coworkers reported that Z-FF-OH (Z: benzyloxycarbonyl) forms coacervate droplets as an intermediate state during nanofiber formation.[37] However, the lifetime of the coacervate is very short (30 min).

(43) Blocher, M.; Liu, D.; Luisi, P. L. Liposome-Assisted Selective Polycondensation of α-Amino Acids and Peptides: the Case of Charged Liposomes. *Macromolecules* **2000**, *33*, 5787–5796.

(44) Izgu, E. C.; Björkbom, A.; Kamat, N. P.; Lelyveld, V. S.; Zhang, W.; Jia, T. Z.; Szostak, J. W. *N*-Carboxyanhydride-Mediated Fatty Acylation of Amino Acids and Peptides for Functionalization of Protocell Membranes. *J. Am. Chem. Soc.* **2016**, *138*, 16669–16676.

(45) Späth, F.; Donau, C.; Bergmann, A. M.; Kränzlein, M.; Synatschke, C. V.; Rieger, B.; Boekhoven, J. Molecular Design of Chemically Fueled Peptide-Polyelectrolyte Coacervate-Based Assemblies. *J. Am. Chem. Soc.* **2021**, *143*, 4782–4789.

(46) Feric, M.; Vaidya, N.; Harmon, T. S.; Mitrea, D. M.; Zhu, L.; Richardson, T. M.; Kriwacki, R. W.; Pappu, R. V.; Brangwynne, C. P. Coexisting Liquid Phases

Underlie Nucleolar Subcompartments. *Cell* **2016**, *165*, 1686−1697.

(47) Cakmak, F. P.; Choi, S.; Meyer, M. O.; Bevilacqua, P. C.; Keating, C. D. Prebiotically-Relevant Low Polyion Multivalency Can Improve Functionality of Membraneless Compartments. *Nat. Commun.* **2020**, *11*, 5949.

(48) Lu, T.; Spruijt, E. Multiphase Complex Coacervate Droplets. *J. Am. Chem. Soc.* **2020**, *142*, 2905–2914.

(49) Kim, S. Y.; Ferrell, J. E., Jr. Substrate Competition as a Source of Ultrasensitivity in the Inactivation of Wee1. *Cell* **2007**, *128*, 1133–1145.

(50) Ferrell, J. E., Jr; Ha, S. H. Ultrasensitivity Part II: Multisite Phosphorylation, Stoichiometric Inhibitors, and Positive Feedback. *Trends Biochem. Sci.* **2014**, *39*, 556–569.

(51) Epstein, I. R.; Xu, B. Reaction-Diffusion Processes at the Nano- and Microscales. *Nat. Nanotechnol.* **2016**, *11*, 312–319.

(52) Ragazzon, G.; Prins, L. J. Energy Consumption in Chemical Fuel-Driven Self-Assembly. *Nat. Nanotechnol.* **2018**, *13*, 882–889.

(53) Rieß, B.; Grötsch, R. K.; Boekhoven, J. The Design of Dissipative Molecular Assemblies Driven by Chemical Reaction Cycles. *Chem* **2020**, *6*, 552–578.

(54) Weißenfels, M.; Gemen, J.; Klajn, R. Dissipative Self-Assembly: Fueling with Chemicals versus Light. *Chem* **2021**, *7*, 23–37.

(55) de Jong, J. J. D.; Hania, P. R.; Pugzlys, A.; Lucas, L. N.; de Loos, M.; Kellogg, R. M.; Feringa, B. L.; Duppen, K.; van Esch, J. H. Light-Driven Dynamic Pattern Formation. *Angew. Chem. Int. Ed.* **2005**, *44*, 2373–2376.

(56) Klajn, R.; Wesson, P. J.; Bishop, K. J. M.; Grzybowski, B. A. Writing Self-Erasing Images Using Metastable Nanoparticle “Inks.” *Angew. Chem. Int. Ed.* **2009**, *48*, 7035–7039.

(57) Pappas, C. G.; Sasselli, I. R.; Ulijn, R. V. Biocatalytic Pathway Selection in Transient Tripeptide Nanostructures. *Angew. Chem. Int. Ed.* **2015**, *54*, 8119–8123.

(58) Boekhoven, J.; Hendriksen, W. E.; Koper, G. J. M.; Eelkema, R.; van Esch, J. H. Transient Assembly of Active Materials Fueled by a Chemical Reaction. *Science* **2015**, *349*, 1075–1079.

(59) Maiti, S.; Fortunati, I.; Ferrante, C.; Scrimin, P.; Prins, L. J. Dissipative Self-

Assembly of Vesicular Nanoreactors. *Nat. Chem.* **2016**, *8*, 725–731.
(60) Ikegami, T.; Kageyama, Y.; Obara, K.; Takeda, S. Dissipative and Autonomous Square-Wave Self-Oscillation of a Macroscopic Hybrid Self-Assembly under Continuous Light Irradiation. *Angew. Chem. Int. Ed.* **2016**, *55*, 8239–8243.
(61) Leira-Iglesias, J.; Tassoni, A.; Adachi, T.; Stich, M.; Hermans, T. M. Oscillations, Travelling Fronts and Patterns in a Supramolecular System. *Nat. Nanotechnol.* **2018**, *13*, 1021–1027.
(62) Jain, A.; Dhiman, S.; Dhayani, A.; Vemula, P. K.; George, S. J. Chemical Fuel-Driven Living and Transient Supramolecular Polymerization. *Nat. Commun.* **2019**, *10*, 450.
(63) Bal, S.; Das, K.; Ahmed, S.; Das, D. Chemically Fueled Dissipative Self-Assembly That Exploits Cooperative Catalysis. *Angew. Chem. Int. Ed.* **2019**, *58*, 244–247.
(64) Chen, R.; Neri, S.; Prins, L. J. Enhanced Catalytic Activity under Non-Equilibrium Conditions. *Nat. Nanotechnol.* **2020**, *15*, 868–874.
(65) Kubota, R.; Makuta, M.; Suzuki, R.; Ichikawa, M.; Tanaka, M.; Hamachi, I. Force Generation by a Propagating Wave of Supramolecular Nanofibers. *Nat. Commun.* **2020**, *11*, 3541.
(66) Panja, S.; Dietrich, B.; Adams, D. J. Chemically Fuelled Self-Regulating Gel-to-Gel Transition. *ChemSystemsChem* **2020**, *2*, e1900038.
(67) Monreal Santiago, G.; Liu, K.; Browne, W. R.; Otto, S. Emergence of Light-Driven Protometabolism on Recruitment of a Photocatalytic Cofactor by a Self-Replicator. *Nat. Chem.* **2020**, *12*, 603–607.
(68) Nakamura, K.; Tanaka, W.; Sada, K.; Kubota, R.; Aoyama, T.; Urayama, K.; Hamachi, I. Phototriggered Spatially Controlled Out-of-Equilibrium Patterns of Peptide Nanofibers in a Self-Sorting Double Network Hydrogel. *J. Am. Chem. Soc.* **2021**, *143*, 19532–19541.
(69) Samperi, M.; Bdiri, B.; Sleet, C. D.; Markus, R.; Mallia, A. R.; Pérez-García, L.; Amabilino, D. B. Light-Controlled Micron-Scale Molecular Motion. *Nat. Chem.* **2021**, *13*, 1200–1206.
(70) Schnitter, F.; Rieß, B.; Jandl, C.; Boekhoven, J. Memory, Switches, and an OR-Port through Bistability in Chemically Fueled Crystals. *Nat. Commun.* **2022**, *13*, 2816.

(71) Selmani, S.; Schwartz, E.; Mulvey, J. T.; Wei, H.; Grosvirt-Dramen, A.; Gibson, W.; Hochbaum, A. I.; Patterson, J. P.; Ragan, R.; Guan, Z. Electrically Fueled Active Supramolecular Materials. *J. Am. Chem. Soc.* **2022**, *144*, 7844–7851.

(72) Howlett, M. G.; Engwerda, A. H. J.; Scanes, R. J. H.; Fletcher, S. P. An Autonomously Oscillating Supramolecular Self-Replicator. *Nat. Chem.* **2022**, *14*, 805–810.

(73) Strulson, C. A.; Molden, R. C.; Keating, C. D.; Bevilacqua, P. C. RNA Catalysis through Compartmentalization. *Nat. Chem.* **2012**, *4*, 941–946.

(74) Qiao, Y.; Li, M.; Booth, R.; Mann, S. Predatory Behaviour in Synthetic Protocell Communities. *Nat. Chem.* **2017**, *9*, 110–119.

(75) Drobot, B.; Iglesias-Artola, J. M.; Le Vay, K.; Mayr, V.; Kar, M.; Kreysing, M.; Mutschler, H.; Dora Tang, T.-Y. Compartmentalised RNA Catalysis in Membrane-Free Coacervate Protocells. *Nat. Commun.* **2018**, *9*, 3643.

(76) Martin, N.; Douliez, J.-P.; Qiao, Y.; Booth, R.; Li, M.; Mann, S. Antagonistic Chemical Coupling in Self-Reconfigurable Host-Guest Protocells. *Nat. Commun.* **2018**, *9*, 3652.

(77) Poudyal, R. R.; Guth-Metzler, R. M.; Veenis, A. J.; Frankel, E. A.; Keating, C. D.; Bevilacqua, P. C. Template-Directed RNA Polymerization and Enhanced Ribozyme Catalysis inside Membraneless Compartments Formed by Coacervates. *Nat. Commun.* **2019**, *10*, 490.

(78) Mason, A. F.; Yewdall, N. A.; Welzen, P. L. W.; Shao, J.; van Stevendaal, M.; van Hest, J. C. M.; Williams, D. S.; Abdelmohsen, L. K. E. A. Mimicking Cellular Compartmentalization in a Hierarchical Protocell through Spontaneous Spatial Organization. *ACS Cent. Sci.* **2019**, *5*, 1360–1365.

(79) Altenburg, W. J.; Yewdall, N. A.; Vervoort, D. F. M.; van Stevendaal, M. H. M. E.; Mason, A. F.; van Hest, J. C. M. Programmed Spatial Organization of Biomacromolecules into Discrete, Coacervate-Based Protocells. *Nat. Commun.* **2020**, *11*, 6282.

(80) Liu, S.; Zhang, Y.; Li, M.; Xiong, L.; Zhang, Z.; Yang, X.; He, X.; Wang, K.; Liu, J.; Mann, S. Enzyme-Mediated Nitric Oxide Production in Vasoactive Erythrocyte Membrane-Enclosed Coacervate Protocells. *Nat. Chem.* **2020**, *12*, 1165–1173.

(81) Liu, J.; Tian, L.; Qiao, Y.; Zhou, S.; Patil, A. J.; Wang, K.; Li, M.; Mann, S.

Hydrogel-Immobilized Coacervate Droplets as Modular Microreactor Assemblies. *Angew. Chem. Int. Ed.* **2020**, *59*, 6853–6859.

(82) Love, C.; Steinkühler, J.; Gonzales, D. T.; Yandrapalli, N.; Robinson, T.; Dimova, R.; Dora Tang, T.-Y. Reversible pH-Responsive Coacervate Formation in Lipid Vesicles Activates Dormant Enzymatic Reactions. *Angew. Chem. Int. Ed.* **2020**, *59*, 5950–5957.

(83) Gobbo, P.; Tian, L.; Pavan Kumar, B. V. V. S.; Turvey, S.; Cattelan, M.; Patil, A. J.; Carraro, M.; Bonchio, M.; Mann, S. Catalytic Processing in Ruthenium-Based Polyoxometalate Coacervate Protocells. *Nat. Commun.* **2020**, *11*, 41.

(84) Le Vay, K.; Song, E. Y.; Ghosh, B.; Dora Tang, T.-Y.; Mutschler, H. Enhanced Ribozyme-Catalyzed Recombination and Oligonucleotide Assembly in Peptide-RNA Condensates. *Angew. Chem. Int. Ed.* **2021**, *60*, 26096–26104.

(85) Iglesias-Artola, J. M.; Drobot, B.; Kar, M.; Fritsch, A. W.; Mutschler, H.; Dora Tang, T.-Y.; Kreysing, M. Charge-Density Reduction Promotes Ribozyme Activity in RNA-Peptide Coacervates via RNA Fluidization and Magnesium Partitioning. *Nat. Chem.* **2022**, *14*, 407–416.

(86) Higashiguchi, K.; Taira, G.; Kitai, J.; Hirose, T.; Matsuda, K. Photoinduced Macroscopic Morphological Transformation of an Amphiphilic Diarylethene Assembly: Reversible Dynamic Motion. *J. Am. Chem. Soc.* **2015**, *137*, 2722–2729.

(87) Garenne, D.; Beven, L.; Navailles, L.; Nallet, F.; Dufourc, E. J.; Douliez, J.-P. Sequestration of Proteins by Fatty Acid Coacervates for Their Encapsulation within Vesicles. *Angew. Chem. Int. Ed.* **2016**, *55*, 13475–13479.

(88) Nakashima, K. K.; Baaij, J. F.; Spruijt, E. Reversible Generation of Coacervate Droplets in an Enzymatic Network. *Soft Matter* **2018**, *14*, 361–367.

(89) Nishida, K.; Tamura, A.; Yui, N. pH-Responsive Coacervate Droplets Formed from Acid-Labile Methylated Polyrotaxanes as an Injectable Protein Carrier. *Biomacromolecules* **2018**, *19*, 2238–2247.

(90) Sato, Y.; Sakamoto, T.; Takinoue, M. Sequence-Based Engineering of Dynamic Functions of Micrometer-Sized DNA Droplets. *Sci. Adv.* **2020**, *6*, eaba3471.

(91) Teders, M.; Pogodaev, A. A.; Bojanov, G.; Huck, W. T. S. Reversible Photoswitchable Inhibitors Generate Ultrasensitivity in Out-of-Equilibrium Enzymatic Reactions. *J. Am. Chem. Soc.* **2021**, *143*, 5709–5716.

TOC graphic

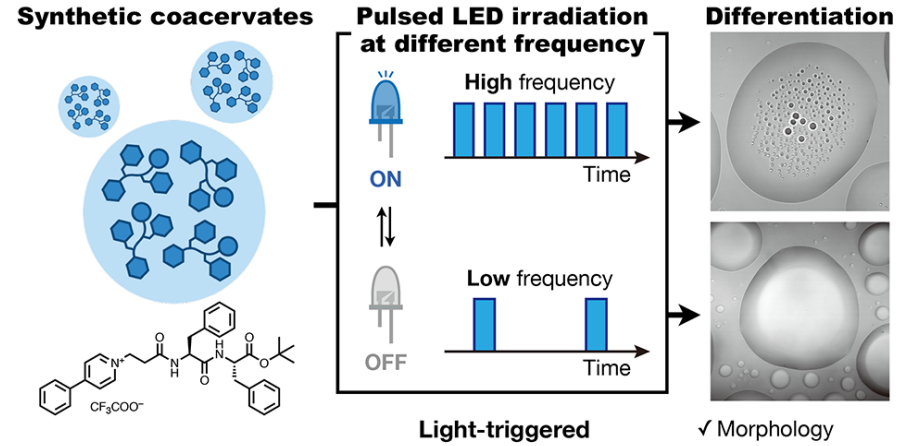
Synthetic coacervates
Pulsed LED irradiation at different frequency
Differentiation
High frequency
Time
ON
OFF
Low frequency
Time
CF3COO⁻
with methacrylate, photo-initiator
Light-triggered radical polymerization
✓ Morphology
✓ Physical properties